# Stability of Polar Vortex Lattice in Ferroelectric Superlattices

Zijian Hong[1], Anoop R. Damodaran[2], Fei Xue[1], Shang-Lin Hsu [2, 3, 4], Jason Britson[1], Ajay K. Yadav[2, 3], Christopher T. Nelson[2,3], Jian-Jun Wang [1], James F. Scott[5], Lane W. Martin[2, 3], Ramamoorthy Ramesh[2, 3, 4,*], Long-Qing Chen[1,#]

[1] Department of Materials Science and Engineering, The Pennsylvania State University, University Park, PA 16802, USA

[2] Department of Materials Science and Engineering, University of California,

Berkeley, CA 94720, USA

[3] Materials Sciences Division, Lawrence Berkeley National Laboratory, Berkeley, CA 94720, USA

[4] Department of Physics, University of California, Berkeley, CA 94720, USA

[5] Schools of Chemistry and Physics, University of St Andrews, St Andrews KY16 9ST, UK

**ABSTRACT**: A novel mesoscale state comprising of ordered polar vortex lattice has been demonstrated in ferroelectric superlattices of $PbTiO_3/SrTiO_3$. Here, we employ phase-field simulations, analytical theory, and experimental observations to evaluate thermodynamic conditions and geometric length scales that are critical for the formation of such exotic vortex states. We show that the stability of these vortex lattices involve an intimate competition between long-range electrostatic, long-range elastic, and short-range polarization gradient-related interactions leading to both an upper- and a lower- bound to the length scale at which these states can be observed. We found that the critical length is related to Pi times the intrinsic domain wall width, which could serve as simple intuitive design rule for the discovery of novel ultrafine topological structures in other ferroic systems.

**KEYWORDS**: Ferroelectric superlattices, ultrafine polar vortex, geometric length scale, phase-field simulations, topological structures by design

---

Corresponding authors:

* Dr. R. Ramesh, Email: rramesh@berkeley.edu

# Dr. L. -Q. Chen, Email: lqc3@psu.edu

Artificial superlattices consisting of repeating layers of multiple solids have attracted broad attention within the solid-state community [1-12]. They offer additional degrees of freedom (beyond conventional "strain engineering") by which one can design multifunctional thin-film materials, wherein unit cells of combinations of solid materials are periodically stacked, often giving rise to novel emergent phenomena [6-8]. Within the realm of complex ferroelectric oxides, for instance in $PbTiO_3/SrTiO_3$ (PTO/STO) superlattices, various novel phenomena and polar domain states have been observed (*e.g.*, "improper ferroelectricity" appears in short period superlattices [10, 11], ordered vortex arrays form in intermediate period superlattices [12], and flux-closure domain structures exist in PTO/STO multilayers and large period superlattices [13], etc.). These states arise from complex interplay of competing energies, including depolarization, polarization/chemical gradients, long-range elastic interactions, and interfacial coupling, which dominate at different length scales and thus produce such exotic thickness-dependent ground states [9, 14].

A vortex is an intriguing topological structure, which attracts broad attention in the scientific community from various perspectives, including a polar vortex in meteorology and astronomy, vortex flow in fluid mechanics, spin spirals and skyrmions in ferromagnetics, etc. Ferroelectric

vortex states (characterized by the continuous rotation of ferroelectric polarization around a vortex core, and analogous to those found in magnetic systems) have been theoretically predicted in ferroelectric nanoparticles and nanodots (often referred as "zero-dimensional ferroelectrics" [15-22]), nanoplatelets [23], nanosheets [24], nanotube [25] and superlattices [11, 26], but long range vortex ordering have not been deterministically isolated in experiments. A breakthrough was recently achieved in superlattices of $(PTO)_n/(STO)_n$ on $DyScO_3$ (DSO) $(110)_o$ substrates which exhibit ordered arrays of vortex for intermediate values of $n$ (~10-16, number of unit cells) [12]. Along with the excitement for emergent functionalities in these vortex states and their technological implications, a number of fundamental questions arise regarding their origin and thermodynamic stability. Here, in this work, we explore the following questions: (1) What are the chemical, electrostatic and mechanical boundary conditions that promote the formation of such a vortex lattice in ferroelectric superlattices? (2) What is the length scale at which the vortex lattice is stable over competing ferroelectric states? and (3) What is the role of the STO layers and how can we engineer new phases by tuning these layers?

In order to address these questions, we employ phase-field modeling in conjunction with a Ginzburg-Landau based analytical model to explore the stability of the vortex structure as a function of superlattice periodicity and STO layer thickness. Over the last two decades, phase-field modeling has been widely employed to study the domain structure and evolution in ferroelectric thin films [27-30], and has also been successfully extended to unveil the domain structures, switching kinetics, phase diagrams, and physical properties for a variety of superlattice systems [31-33]. In the phase-field approach, the spatially-dependent polarization vector $\vec{P}$ = ($P_x$, $P_y$, $P_z$) is selected as the order parameter to describe the polar states. The evolution of this polarization is governed by the time-dependent Ginzburg-Landau (TDGL)

equations and driven by the minimization of the total energy, comprised of chemical, elastic, electric, and polarization gradient energies [28]. An iterative, perturbation method is adopted to accommodate for the elastic anisotropy and inhomogeneity of the PTO and STO layers when solving the mechanical equilibrium equations [34]. The calculation details, as well as the related parameters, can be found in literature [27, 35-38] and are further explained in the supplementary materials [39].

We start by exploring the phase-field simulation results for a $(PTO)_{10}/(STO)_{10}$ superlattice coherently strained to a DSO $(110)_o$ substrate (the psuedocubic lattice parameter of PTO, STO is set as 3.957 Å and 3.905 Å, respectively [35, 36]; while the anisotropic in-plane lattice constant for DSO is set as 3.952 and 3.947 Å [38]) – a model system that has demonstrated ordered vortex arrays in previous experiments [12]. It is easily seen that the calculated polarization distribution (Fig. 1a) in the PTO layers mimics the ordered vortex lattice. The zoom-in of a single vortex in the PTO layer clearly shows the continuous rotation of polarization vectors surrounding the vortex center (Fig. 1b), which is experimentally confirmed by the high resolution transmission electron microscopy (HRTEM) polar vector mapping [12, 39]. Both the simulation and experimental results indicate that the size of each vortex is 4-5 nm for this particular superlattice periodicity. We also note that in contrast to the flux-closure polarization structures [13, 40-42], where abrupt polarization changes occur only near the distinct domain wall area, the vortex structures exhibit a continuously rotating polarization. The vortex state is distinctly different and represents a highly inhomogeneous polarization mode that is characterized by a one-dimensional singularity at the vortex core as against two-dimensional domain walls that appear in the flux-closure structures. The vortex core structure in the ferroelectric system is unique as compared to the topologically-protected vortex core in magnetic systems, since the magnitude of polarization

exhibits a huge decrease near the core due to the strong anisotropy in the ferroelectric system. Furthermore, a planar section (Fig. 1c) of the PTO layer reveals that the vortices form long chains along the axial direction, often intersecting other vortices in a classic dislocation-like pattern, and in excellent agreement with planar section TEM studies [12]. A magnified view of this planar section (Fig. 1d) shows the in-plane polarization of neighboring vortices pointing tail-to-tail, and separated by an out-of-plane polarization region confirming the anti-rotation relationship between neighboring vortex pairs throughout the axial direction.

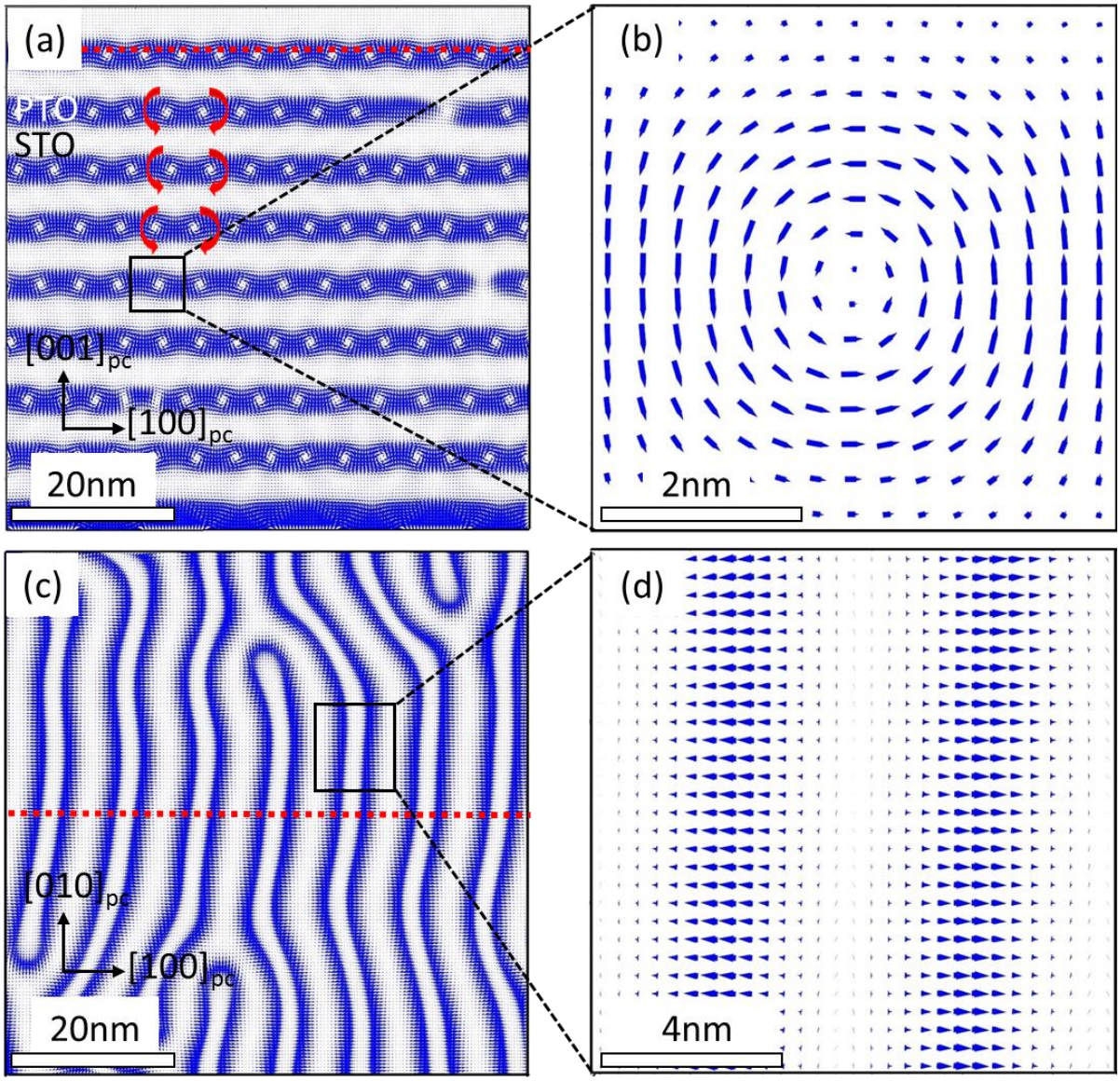


Figure 1. Polarization vector maps for vortices in the $(PTO)_{10}/(STO)_{10}$ superlattice system, calculated from phase-field simulation. (a) Spatial distribution of polarization in the cross-section $(010)_{pc}$ plane, showing the vortex/antivortex structures. (b) Zoom-in result for a single vortex showing the continuous rotation of the polarization vector. (c) Planar view of the PTO layer, showing vortex line arrangement (d) Zoom-in of the vortex line. Dotted line in (a) and (c) show the planes where the planar view and cross-section view are plotted, respectively.

Having confirmed the vortex structure, in order to find the intrinsic thermodynamic stability region for the vortex states, we analytically predict the emergence of the vortex state following references [43-45]. Using the variation of the total free energy with respect to $P_x$, one can explicitly deduce a relationship between the vortex aspect ratio $r$ (ratio of vortex in-plane size $d$ to the superlattice periodicity $a_f$ ) and the superlattice periodicity [39]:

$$\frac{1}{r^2}+1=\frac{a_f^2}{a_0^2} \tag{1}$$

where $a_0$ is the "characteristic length" related to the gradient energy coefficients and the modified Landau coefficients, which can also be estimated by the width of the 180° domain wall $\delta$, $a_0 \sim \pi\delta/\sqrt{2}$ [39]. At room temperature, for short period PTO/STO superlattices, a rough estimation gives a value of ~3.2 nm for the "characteristic length". Since the shape of the vortex is largely controlled by the aspect ratio $r$, we plot it as a function of superlattice periodicity (Fig. 2). It can be seen that the aspect ratio decreases with increasing periodicity from both Eq. 1 and the phase-field simulation results. Compared with the vortex pattern in $(PTO)_{10}/(STO)_{10}$ superlattices (Fig. 1b and c), the vortex core in $(PTO)_{20}/(STO)_{20}$ (left inset, Fig. 2) is more elongated along the thickness direction than that in $(PTO)_{10}/(STO)_{10}$, and it further elongates to resemble a classic 180° domain wall in a $(PTO)_{27}/(STO)_{27}$ superlattice (right inset, Fig. 2). The elongation of the vortex core with increasing size has also been captured experimentally by TEM polar mapping of $(PTO)_{16}/(STO)_{16}$ superlattice [30] and is shown in previous two-dimensional phase-field simulations [46].

Based on Eq. 1, in order to ensure the physical sense for the vortex state, $a_f$ and $a_0$ must satisfy:

$$a_f \geq a_0 \tag{2}$$

Correspondingly, for superlattice periodicities where $a_f < a_0$ (*i.e.*, for n ≤ 9) the vortex state is unstable and inplane domains form. The upper bound for the vortex lattice is obscure due to the continuous nature of the vortex to flux-closure transition, while we can estimate an empirical critical aspect ratio of ~0.3 (Fig. 2), below which the circular vortex core becomes a classic 180° domain wall. The condition for stabilizing the vortex structure can be derived by combining the lower boundary from Eq. 2:

$$a_0 \leq a_f \leq \sqrt{12} a_0 \tag{3}$$

Practically, the smooth circular-like rotation pattern can be expected where：

$$a_f \sim \sqrt{2} a_0 \sim \pi\delta \tag{4}$$

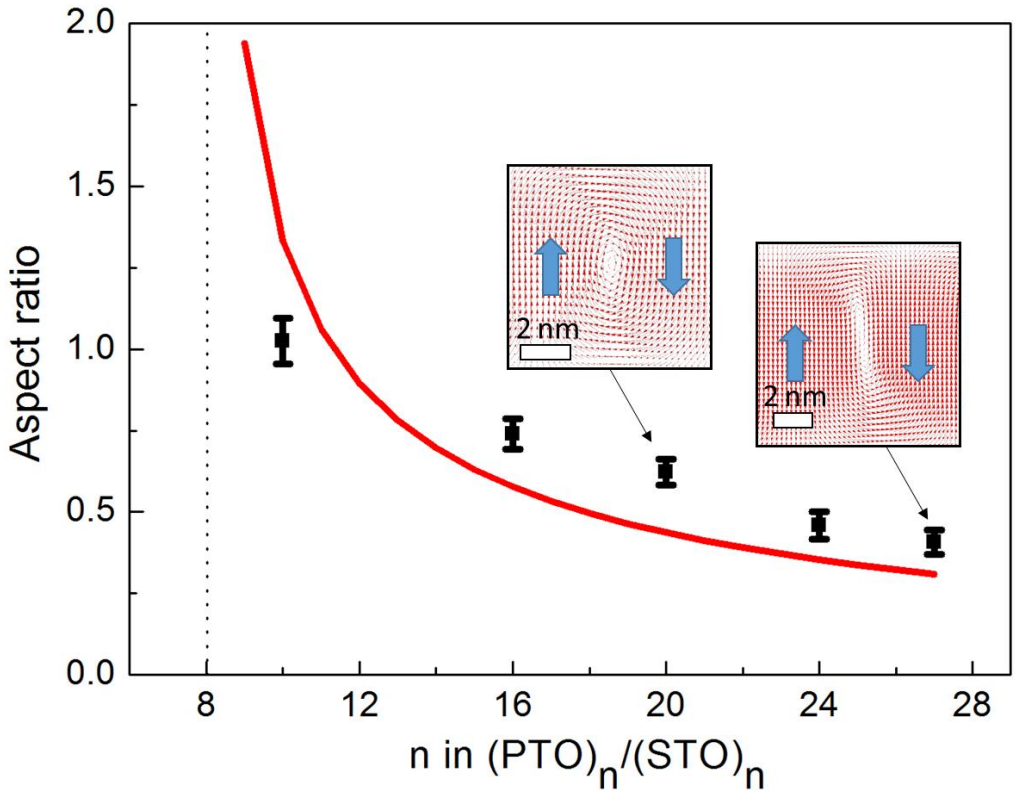


Figure 2. "Vortex" aspect ratio as a function of superlattice periodicity. The red curve is calculated according to Eq. 1, where a value of 8 unit cells is used for $a_0$. The square data points and error bars are results calculated from phase-field simulations. The left and right insets are the simulated domain structures for $(PTO)_{20}/(STO)_{20}$ and $(PTO)_{27}/(STO)_{27}$, respectively. The dash line shows criterion 2.

Eqs 3 and 4 give the condition on the range of superlattice periodicity for which vortex structure may be expected. In order to observe a nano-scale vortex structure, the "characteristic length" $a_0$, which can be estimated by the 180° domain wall width of the bulk crystal, should be some intermediate value. If it is too small, the stability window given by Eq. 3 will be too small so that this structure cannot be captured. On the other hand, a large $a_0$ leads to an increase in the threshold transition length, where dramatic increase of polarization rotation region would lead to a large increase in gradient energy; which will favor the simple *a*/*c*-type structure. It is

worthwhile pointing out that Eq. 4 bridges the stability of mesoscale vortex with intrinsic bulk ferroelectric material properties (i.e., domain wall width) that serves as an intuitive simple design rule for the discovery of vortex and other possible topological structures. It is also discovered that this rule not only works well for the current PTO/STO system and other low-dimensional PTO nanostructures, but also serves as a generally good estimation for the length scale of vortex or vortex-like structures in other ferroelectric materials, *e.g.*, $BaTiO_3$ (see Refs. 47 and 48 for the sizes of the vortex or vortex-like structure in rhombohedral and orthorhombic phases, the domain wall width is given by Ref. 49) and $BiFeO_3$ (see Ref. 50 for the size of vortex-like structure and Ref. 51 for the domain wall width).

The temperature effect can also be described by Eq. 3. With increasing temperature, the "characteristic length" increases, giving rise to an upward shift of the phase boundary between the $a_1/a_2$ twin domains and vortex state. As a result, for a given periodicity, e.g., $(PTO)_{16}/(STO)_{16}$, a phase transition from vortex to $a_1/a_2$ twins can be expected when temperature increases; such temperature-dependent phase transition was found by recent experimental results [52]. Further reducing of the aspect ratio also indicates a lowering of symmetry, which resembles the decrease of *k* value as shown in Lukyanchuk *et al.*, where the shape of polarization domain changes from polyhedron-like to triangular-like [53].

To better understand the nature of length-scale effects, we explored the evolution of the polar state of the PTO layer as a function of superlattice periodicity through integrated theoretical-experimental observations. As revealed in Fig. 3, with increasing superlattice period, the total energy density of the lowest energy state is monotonically decreased. The higher total energy density at lower superlattice periodicity is related to decreased benefits from the Landau chemical energy and indicative of a decreased stability of the ferroelectric state. In this regime of

length scales (up to n = 10), strong depolarization effects drive a completely in-plane polarized ferroelectric $a_1/a_2$ twin-domain structure (top-left inset, Fig. 3) over the elastically preferred *c*/*a* domain structure (corresponding to the domain structure observed in thick PTO film under strain condition from the DSO $(110)_o$ substrate [54]), as revealed by both phase-field simulation and planar and cross-section TEM (supplementary materials). At superlattice period $n>=10$ (length scale of ~4 nm), it becomes feasible to introduce these gradients to adopt configurations that allow further lowering of the chemical and elastic energy density at the expense of increased gradient energy contributions. This sets the lower-bound for the observation of vortex states in the system. Consequently, for superlattice period $n>=10$, it adopts ordered configurations that involve an intimate competition between long-range elastic and electrostatic, as well as short-range polarization gradient effects. Thus, with increasing period from n $\approx$10 to n $\approx$ 16, we see that the vortex state (middle inset, Fig. 3) becomes favorable, and we predict a phase transition from the in-plane polarized $a_1/a_2$ ferroelectric phase to an ordered vortex lattice. On the other hand, the transition from a vortex to a flux-closure domain structure (bottom inset, Fig. 3) at large superlattice periodicity is continuous and a more subtle one.

From the energy point of view, the formation of a vortex at short-to-intermediate periods (*e.g.*, n$\approx$10 to n$\approx$16) can be understood as a result of a balance between the individual energies: the combined effect of elastic and electric energies favors mixtures of in-plane and out-of-plane polarization, whereas the gradient energy is lower in the smooth rotating configuration (*i.e.*, vortex) as compared to the structure with distinct domain walls (*e.g.*, flux-closure) at short periods. The higher gradient energy in the flux-closure compared to vortex at lower periods can be understood, since the gradient energy density is much larger near the conventional domain

walls (*e.g.*, 180° and 90° walls in the tetragonal system) as compared to the smooth polarization rotation pattern in a vortex structure.

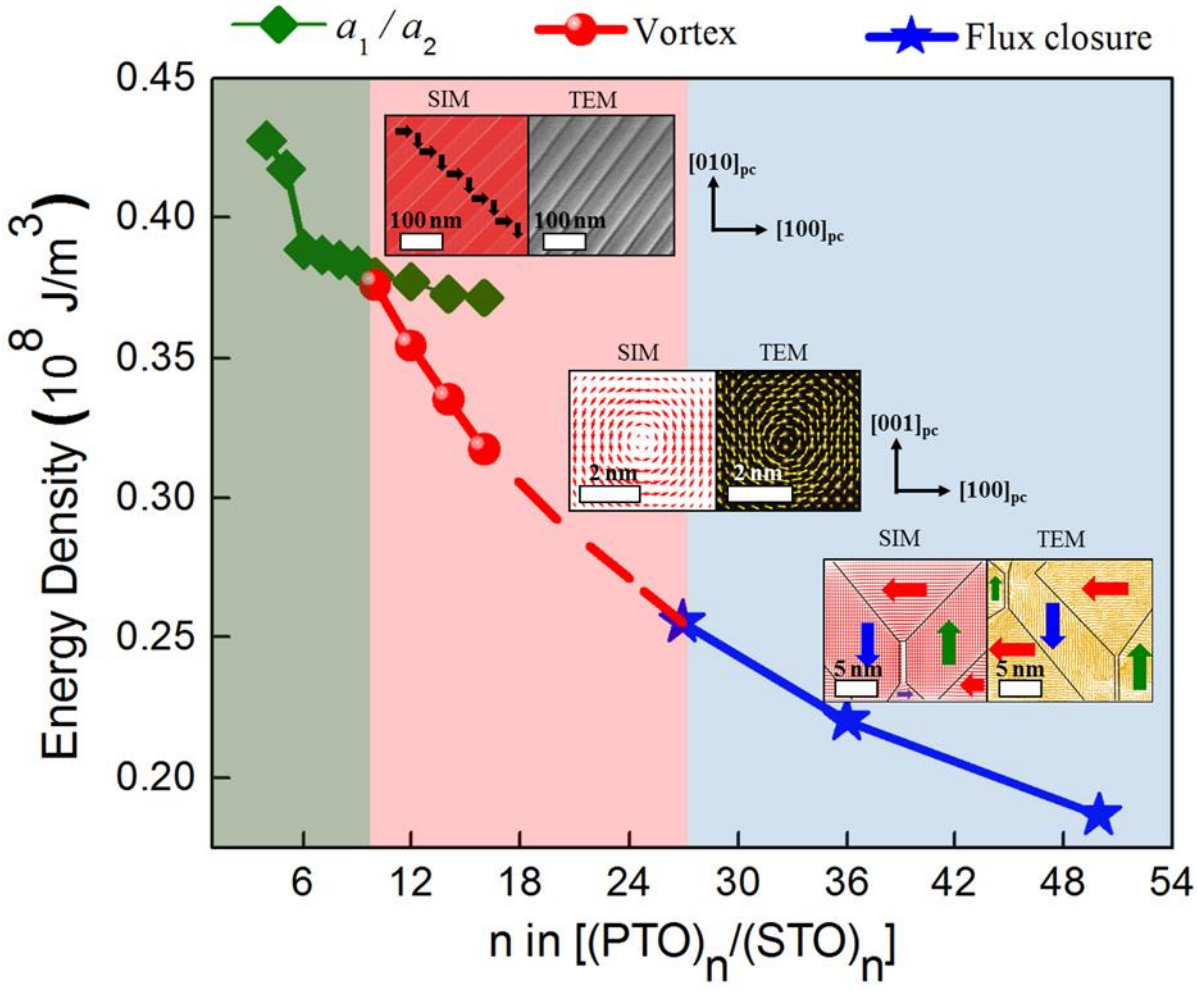


Fig.3 Phase diagram and total energy density for the $(PTO)_n/(STO)_n$ superlattice grown on the DSO substrate, as calculated by the phase-field simulations and verified experimentally. Inset: top left shows the simulation and planar TEM result of in-plane view of $a_1a_2$ twin domain structure for n=6; middle left and right are the vortex structure for n=10 from simulation and experimental TEM mapping, respectively; The bottom left and right inset are the cross-section of flux-closure structure for n=50 from phase-field simulation and experimental TEM vector mapping, respectively. "SIM" and "TEM" stands for simulation, and transmission electron microscopy data.

To further explore the role of the insulating STO layers, a phase diagram with varying STO layer thickness (*i.e.*, $(PTO)_{10}/(STO)_m$) and the analysis of the electric energy density of the two layers are calculated by the phase-field method, as shown in Fig. 4. With thin STO layers (*e.g.*, m=2) between the PTO layers, STO is highly polarized by the PTO layers due to the large internal field. As a consequence, the electric energy density inside the STO layer is highly negative, which comes at the cost of higher electric energy in the PTO layer. The significant polarization inside the STO layers serves as the bridge that connects the PTO layers and hence an *a*/*c* twin structure forms, similar to the domain pattern for a PTO thin film grown on a DSO substrate, which form to lower the elastic energy of the PTO layers. The polar phase of STO has been observed recently in both experiment and theory with a polarization up to 0.3 $C/m^2$ in ultrathin film [55]. Upon increasing the STO layer thickness there is a monotonic decrease of the average polarization as well as the internal field inside the STO layer, which increases the electric energy density of the STO layer. Whereas, in order to decrease the polar discontinuity at the interface, the vortex state is formed. The vortex state is often mixed with other phases (i.e., *a*/*c* with thin STO layers while $a_1/a_2$ at thick STO layers) to reduce the elastic/electric energies. As a result, the average electric energy of the PTO layer hits a plateau. Further increasing of the STO thickness could lead to increasing of the depolarization strength, which will eventually leads to the formation of $a_1/a_2$ twin structure in an attempt to further reduce the electric and gradient energy of the PTO layer at the expense of increased elastic energy.

Ultimately, the importance of the STO layers can be addressed as follows: the polarizability of these layers could be used to easily tune the polar discontinuity as well as the strength of the depolarization field, in combination with the size effect. The stability of the ground state polar vortex phase is strongly influenced by the depolarization strength, the variation of which could

lead to a rich phase diagram. In general, lowering the electric energy at higher depoling strength leads to complete inplane polarization (*i.e*, $a_1/a_2$), while lower depoling strength leads to the formation of out-of-plane domains (*i.e.*, *a*/*c* and even $c^+/c^-$). Thus, it is more feasible to choose weak ferroelectrics (or improper ferroelectrics) instead of pure paraelectric material to design tunable domain structure and properties by engineering the thickness or composition of these layers.

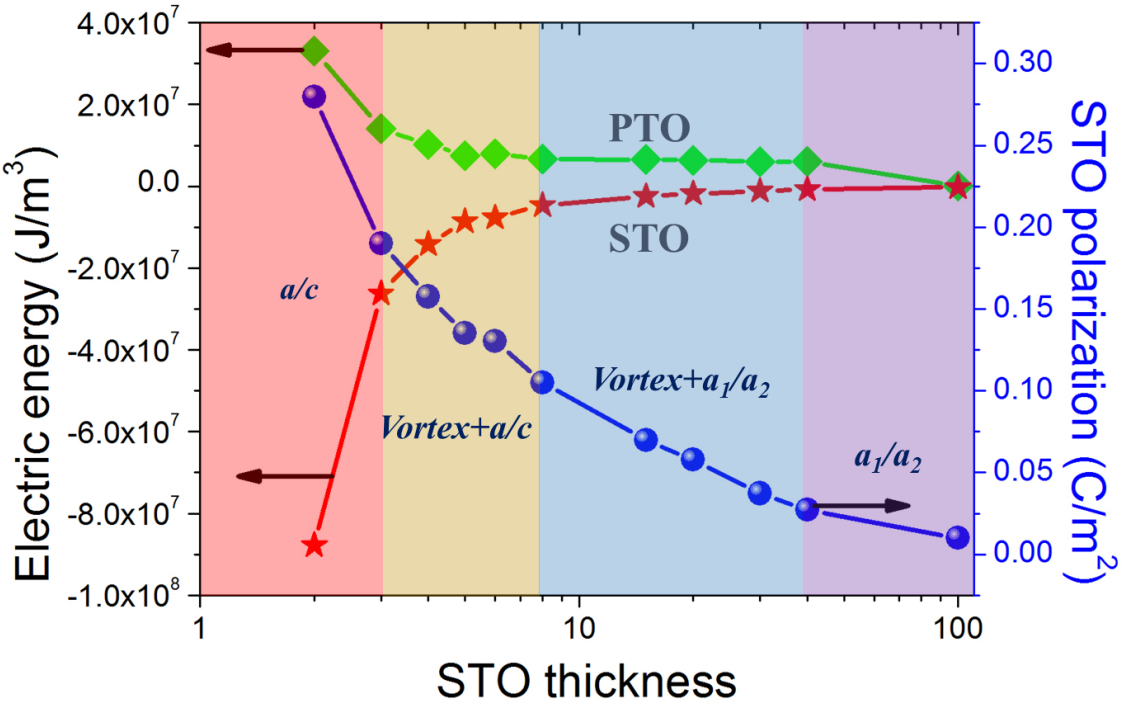


Fig.4 Phase diagram, STO polarization and average electric energy density for the $(PTO)_{10}/(STO)_n$ superlattice grown on the DSO substrate, as calculated by the phase-field simulations, showing the existence of *a*/*c*, vortex mixtures and $a_1/a_2$.

In summary, we have established that vortex lattices can be stabilized at intermediate length scale in a paraelectric/ferroelectric superlattices by manipulating the electrical-chemical-mechanical energy contributions. We first propose an analytical analysis, which provides a

design rule to help identify the theoretical stability range of the vortex lattices, where an appropriate "characteristic length" related to the bulk domain wall width is required. The role of each individual contribution in the formation of a vortex state is studied by calculating a size-dependent phase diagram. It is shown that elastic energy favors out-of-plane polarization of the superlattice while the electric energy (in particular the depolarization energy) tries to keep polarization in-plane. Meanwhile, electric energy prefers small spatial spacing between the vortices whereas the polarization gradient energy favors uniform polarization or smooth polarization rotation and thus large spacing between vortices. These competing interactions lead to a transition from $a_1/a_2$ twin polar states, to vortex lattice, and eventually to flux-closure lattices with increasing superlattice periodicity. Whereas the role of STO layers are further explored within the $(PTO)_{10}/(STO)_n$ phase diagram, which indicate that the tunable depoling strength could help engineer multiple phases, while the existence of a weak ferroelectricity in the STO layer could facilitate the formation of the vortex lattice. Thus, our work not only contributes to the further understanding of domain formation mechanism in current $(PTO)_n/(STO)_n$ superlattice system, but also stimulates future studies on developing superlattice-based novel material structures.

## ASSOCIATED CONTENT

### Supporting Information.

The following chapters are contained in the supplementary: descriptions of phase-field methodology; initial setup and simulation parameters; energy density plot of vortex and flux-closure structure: the contribution from elastic, electric, Landau and gradient energies; analytical

expression for the periodicity dependence; synthesis and characterization of superlattice thin films.

## AUTHOR INFORMATION

### Corresponding Authors

*E-mail: Dr. Long-Qing Chen lqc3@psu.edu

Dr. R. Ramesh, Email: rramesh@berkeley.edu

### Acknowledgements

The work is supported by U.S. Department of Energy, Office of Basic Energy Sciences, Division of Materials Sciences and Engineering under Award FG02-07ER46417 (LQC, FX & JB). ZJH acknowledges the support by NSF-MRSEC grant number DMR-1420620 and NSF-MWN grant number DMR-1210588. A.R.D. acknowledges support from the Army Research Office under grant W911NF-14-1-0104. L.W.M. acknowledges support from the National Science Foundation under grant Grant DMR-1451219. A.K.Y., C.T.N. and R.R. acknowledge support from the Office of Basic Energy Sciences, U.S. Department of Energy under contract no. DE-AC02-05CH11231. L.W.M. and R.R. acknowledge support from the Gordon and Betty Moore Foundation's EPiQS Initiative, Grant GBMF5307.

### References

[1] L. Esaki and L. L. Chang, *Phys. Rev. Lett.* **33**, 495 (1974).

[2] I. Chowdhury, R. Prasher, K. Lofgreen *et al.*, *Nature Nanotech.* **4**, 235 - 238 (2009).

[3] S. Smadici, P. Abbamonte, A. Bhattacharya *et al.*, *Phys. Rev. Lett.* **99**, 196404 (2007).

[4] J. Sinsheimer, S. J. Callori, B. Bein, Y. Benkara, J. Daley, J. Coraor, D. Su, P. W. Stephens, and M. Dawber, *Phys. Rev. Lett.* **109**, 167601 (2012).

[5] H. N. Lee, H. M. Christen, M. F. Chisholm, C. M. Rouleau, and D. H. Lowndes, *Nature (London)* **433**, 395 (2005).

[6] M. Dawber, C. Lichtensteiger, M. Cantoni, M. Veithen, P. Ghosez, K. Johnston, K. M. Rabe, and J.-M. Triscone, *Phys. Rev. Lett.* **95**, 177601 (2005).

[7] M. Dawber, N. Stucki, C. Lichtensteiger, S. Gariglio, P. Ghosez, J.-M. Triscone, *Adv. Mater.* **19**, 4153 (2007).

[8] D. G. Schlom, L.-Q. Chen, C. J. Fennie, V. Gopalan, D. A. Muller, X. Q. Pan, R. Ramesh, and R. Uecker, *MRS Bulletin* **39(02)**, 118-130 (2014).

[9] V. A. Stephanovich, I. A. Luk'yanchuk, and M. G. Karkut, *Phys. Rev. Lett.* **94**, 047601 (2005).

[10] E. Bousquet, M. Dawber, N. Stucki, C. Lichtensteiger, P. Hermet, S. Gariglio, J.-M. Triscone, and P. Ghosez, *Nature (London)* **452**, 732 (2008).

[11] P. Aguado-Puente and J. Junquera. *Phys. Rev. B* **85**, 184105 (2012).

[12] A. K. Yadav, C. T. Nelson, S. L. Hsu, Z. Hong, J. D. Clarkson, C. M. Schlepütz, A. R. Damodaran, P. Shafer, E. Arenholz, L. R. Dedon, D. Chen, A. Vishwanath, A. M. Minor, L. Q. Chen, J. F. Scott, L. W. Martin & R. Ramesh, *Nature (London)*, **530**, 198–201 (2016).

[13] Y. L. Tang, Y. L. Zhu, X. L. Ma, A. Y. Borisevich, A. N. Morozovska, E. A. Eliseev, W. Y.Wang, Y. J. Wang, Y. B. Xu, Z. D. Zhang, and S. J. Pennycook, *Science* **348**, 547–551 (2015).

[14] A. R. Balakrishna and J. E. Huber, *Appl. Phys. Lett.***106**, 092906 (2015).

[15] S. Prosandeev, I. Ponomareva, I. Naumov, I. Kornev and L. Bellaiche, *J. Phys.: Condens. Matter* **20**, 193201 (2008).

[16] I. I. Naumov, L. Bellaiche, and H. Fu, *Nature (London)* **432**, 737 (2004).

[17] P. Aguado-Puente and J. Junquera, *Phys. Rev. Lett.* **100**, 177601 (2008).

[18] D. Sichuga and L. Bellaiche, *Phys. Rev. Lett.* **106**, 196102 (2011).

[19] B. J. Rodriguez, X. S. Gao, L. F. Liu, W. Lee, Naumov, Ii, A. M. Bratkovsky, D. Hesse, and M. Alexe, *Nano Lett.*, **9(3)**, 1127-1131 (2009).

[20] B. Lee, S. M. Nakhmanson, and O. Heinonen, *Appl. Phys. Lett.* **104 (26)**, 262906 (2014).

[21] J. M. Gregg, *Ferroelectrics*, **433**, 74-87 (2012).

[22] J. Wang, *Appl. Phys. Lett.*, **97(19)**, 192901, 2010.

[23] W. J. Chen, Y. Zheng, and B. Wang, *Sci. Rep.* **2**, 796 (2012).

[24] W. J. Chen, Y. Zheng, and B. Wang, *Appl. Phys. Lett.*, **100(6)**, 062901 (2012).

[25] J. Wang, M. Kamlah, *Phys. Rev. B* **80 (1)**, 012101 (2009).

[26] P. Aguado-Puente, P. García-Fernández, and J. Junquera, *Phys. Rev. Lett.* **107**, 217601 (2011).

[27] Y. L. Li, S. Y. Hu, Z. K. Liu, and L.-Q. Chen, *Acta Mater.* **50**, 395-411 (2002).

[28] L.Q. Chen, *J. Am. Ceram. Soc.* **91**, 1835–1844 (2008).

[29] Z. J. Hong, J. Britson, J.-M. Hu, L. Q. Chen, *Acta Mater.*, **73**, 75-82 (2014).

[30] C. M. Wu, W. J. Chen, Y. Zheng, D. C. Ma, B. Wang, J. Y. Liu, and C. H. Woo, *Sci. Rep.*, **4**, 3946 (2014).

[31] W. Tian, J. C. Jiang, X. Q. Pan, J. H. Haeni, Y. L. Li, L. Q. Chen, D. G. Schlom, J. B. Neaton, K. M. Rabe, and Q. X. Jia, *Appl. Phys. Lett.*, **89 (9)**, 092905 (2006).

[32] P. P. Wu, X. Q. Ma, Y. L. Li, V. Gopalan, and L. Q. Chen, *Appl. Phys. Lett.*, **100(9)**, 092905 (2012).

[33] L. Hong, P. P. Wu, Y. L. Li, V. Gopalan, C.-B. Eom, D. G. Schlom, and L.-Q. Chen, *Phys. Rev. B*, **90(17)**, 174111 (2014).

[34] J. J. Wang, X. Q. Ma, Q. Li, J. Britson, and L. Q. Chen, *Acta Mater.*, **61(20)**, 7591 (2013).

[35] M. J. Haun, E. Furman, S. J. Jiang, H. A. McKinstry, and L. E. Cross, *J. Appl. Phys.* **62**, 3331-3338 (1987).

[36] G. Sheng, Y. L. Li, J. X. Zhang, S. Choudhury, Q. X. Jia, V. Gopalan, D. G. Schlom, Z. K. Liu and L. Q.

Chen, *Appl. Phys. Lett.* **96**, 232902 (2010).

[37] Z. H. Chen, A. R. Damodaran, R. Xu, S. Lee, L. W. Martin, *Appl. Phys. Lett.* **104**, 182908 (2014).

[38] A. K. Tagantsev, *Ferroelectrics* **375**, 19-27 (2008).

[39] Supplementary materials.

[40] Y. Ivry, D. P. Chu, J. F. Scott, and C. Durkan, Phys. Rev. Lett. 104(20), 207602 (2010).

[41] C. L. Jia, K. W. Urban, M. Alexe, D. Hesse, and I. Vrejoiu, Science, 331, 1420-1423 (2011).

[42] C. T. Nelson, B. Winchester, Y. Zhang, S. J. Kim, A. Melville, C. Adamo, C. M. Folkman, S. H. Baek, C. B. Eom, D. G. Schlom, L. Q. Chen, and X. Q. Pan, Nano Lett.,11(2), 828-834 (2011).

[43] I. A. Luk'yanchuk, L. Lahoche, and A. Sene´, *Phys. Rev. Lett.* **102**, 147601 (2009).

[44] V.A. Stephanovich, I.A. Luk'yanchuk, M.G. Karkut, *Phys. Rev. Lett.* **94**, 047601 (2005).

[45] A. P. Levanyuk and I. B. Misirlioglu, *J. Appl. Phys.* **119**, 024109 (2016).

[46] Z. D. Zhou and D. Y. Wu, *AIP Advances* **5**, 107206 (2015).

[47] V. Stepkova, P. Marton, N. Setter, and J. Hlinka, *Phys. Rev. B* **89**, 060101(R) (2014).

[48] Z. Gui, L. Wang, and L. Bellaiche, *Nano Lett.*, **15**, 3224 −3229 (2015).

[49] P. Marton, I. Rychetsky, and J. Hlinka, *Phys. Rev. B* **81**, 144125 (2010).

[50] W. Ren and L. Bellaiche, *Phys. Rev. Lett.* **107**, 127202 (2011).

[51] Y. Wang, C. Nelson, A. Melville, B. Winchester, S. Shang, Z. Liu, D. G. Schlom, X. Pan, and L. –Q. Chen, *Phys. Rev. Lett.* **110**, 267603 (2013).

[52] A. R. Damodaran, *et al., In Preparation*.

[53] I. A. Luk'yanchuk, P. Sharma, T. Nakajima, S. Okamura, J. F. Scott, and A. Gruverman, *Nano Lett.* **14**, 6931–6935 (2014).

[54] Q. Y. Qiu, V. Nagarajan, and S. P. Alpay, *Phys. Rev. B*, **78**,064117 (2008).

[55] D. Lee, H. Lu, Y. Gu, S.-Y. Choi, S.-D. Li, S. Ryu, T. R. Paudel, K. Song, E. Mikheev, S. Lee, S. Stemmer, D. A. Tenne, S. H. Oh, E. Y. Tsymbal, X. Wu, L.-Q. Chen, A. Gruverman, C. B. Eom, Science, **349**, 1314–1317 (2015).

Table of Contents Graphic (For Table of Contents Only)